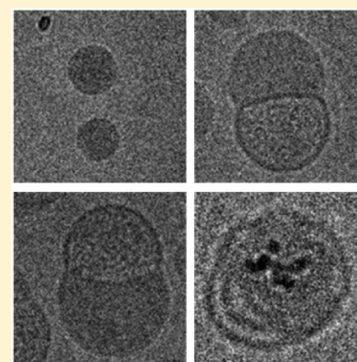


Microfluidic Mixing: A General Method for Encapsulating Macromolecules in Lipid Nanoparticle Systems

Alex K. K. Leung, Yuen Yi C. Tam, Sam Chen, Ismail M. Hafez, and Pieter R. Cullis*

Department of Biochemistry and Molecular Biology, The University of British Columbia, Vancouver, British Columbia, Canada V6T 1Z3

ABSTRACT: Previous work has shown that lipid nanoparticles (LNP) composed of an ionizable cationic lipid, a poly(ethylene glycol) (PEG) lipid, distearoylphosphatidylcholine (DSPC), cholesterol, and small interfering RNA (siRNA) can be efficiently manufactured employing microfluidic mixing techniques. Cryo-transmission electron microscopy (cryo-TEM) and molecular simulation studies indicate that these LNP systems exhibit a nanostructured core with periodic aqueous compartments containing siRNA. Here we examine first how the lipid composition influences the structural properties of LNP–siRNA systems produced by microfluidic mixing and, second, whether the microfluidic mixing technique can be extended to macromolecules larger than siRNA. It is shown that LNP–siRNA systems can exhibit progressively more bilayer structure as the proportion of bilayer DSPC lipid is increased, suggesting that the core of LNP–siRNA systems can exhibit a continuum of nanostructures depending on the proportions and structural preferences of component lipids. Second, it is shown that the microfluidic mixing technique can also be extended to encapsulation of much larger negatively charged polymers such as mRNA (1.7 kb) or plasmid DNA (6 kb). Finally, as a demonstration of the generality of the microfluidic mixing encapsulation process, it is also demonstrated that negatively charged gold nanoparticles (5 nm diameter) can also be efficiently encapsulated in LNP containing cationic lipids. Interestingly, the nanostructure of these gold-containing LNP reveals a “currant bun” morphology as visualized by cryo-TEM. This structure is fully consistent with LNP–siRNA structure predicted by molecular modeling.



1. INTRODUCTION

Lipid nanoparticle (LNP) and polymer-based systems have proven potential for delivery of small molecules and macromolecules such as siRNA.^{1–3} Previous work has shown that highly potent LNP–siRNA systems can self-assemble from mixtures of ionizable cationic lipids, PEG lipids, DSPC, and cholesterol formulated with siRNA using a herringbone micromixer.^{4,5} These LNP exhibit siRNA encapsulation efficiencies approaching 100% and a uniformly electron dense interior as observed by cryo-TEM. Molecular modeling and experimental data indicate that these LNP have a nanostructured core consisting of inverted micellar structures containing siRNA.⁶ In contrast, LNP systems formed (using a different formulation technique) from lipid mixtures with a higher proportion of the bilayer forming lipid DSPC and containing antisense oligonucleotides exhibit small multilamellar structures where the oligonucleotides are apparently entrapped between concentric bilayers of lipid.⁷ These results suggest the possibility that LNP formulations of oligonucleotides can adopt a variety of structures depending on the proportions of component lipids.

In this work we investigate, employing cryo-TEM techniques, the structural properties of LNP–siRNA systems formed using the microfluidic technique and containing different proportions of lipids. It is shown that a continuum of structures can be observed depending on the lipid composition and the siRNA content. Further, we investigate the possibility that the technique for encapsulating macromolecules such as siRNA

can be extended to provide efficient encapsulation of larger negatively charged macromolecules such as mRNA, plasmid, or colloidal gold. It is shown that highly efficient encapsulation of all these macromolecules can be achieved using the microfluidic mixing technique. Of note, the structural features exhibited by LNP containing gold nanoparticles provide strong support for the inverted micellar nanostructured core proposed in previous work.⁶

2. MATERIALS AND METHODS

2.1. Materials. The lipids 1,2-dioleoyl-*sn*-glycero-3-phosphorylethanolamine (DOPE) and 1,2-distearoyl-*sn*-glycero-3-phosphorylcholine (DSPC) were obtained from Avanti Polar Lipids (Alabaster, AL). The ionizable cationic lipid 2,2-dilinoleyl-4-(2-dimethylaminoethyl)-1,3-dioxolane (DLin-KC2-DMA) and *N*-[(methoxypoly(ethylene glycol) 2000 carbamyl]-1,2-dimyristyloxpropyl-3-amine (PEG-c-DMA) were obtained from Acuitas Therapeutics Inc. (Vancouver, BC). Cholesterol, sodium acetate, and sodium citrate tribasic were obtained from Sigma-Aldrich (St. Louis, MO). 2-(*N*-Morpholino)-ethanesulfonic acid (MES) was obtained from BDH (Westchester, PA). The Cholesterol E Total Cholesterol assay kit was obtained from Wako Diagnostics (Richmond, VA). Negatively

Received: March 26, 2015

Revised: June 15, 2015

Published: June 18, 2015



charged, tannic acid-capped gold nanoparticles were purchased from Ted Pella, Inc. (Redding, CA). The Quant-it RiboGreen RNA assay kit was obtained from Molecular Probes (Eugene, OR).

2.2. Encapsulation of Nucleic Acids. LNP were prepared by mixing appropriate volumes of lipid stock solutions in ethanol with an aqueous solution of oligonucleotide employing a microfluidic micromixer as described elsewhere.⁵ A staggered herringbone micromixer⁸ was employed. The mixing channel is 200 μm wide and 79 μm high, and the herringbones are 31 μm high and 50 μm thick.^{4,5} All oligonucleotides were dissolved in 25 mM sodium acetate buffer, pH 4.0. Lipid dissolved in ethanol and 3 volumes of nucleic acids in buffer were combined in the microfluidic micromixer using a dual-syringe pump (PHD Ultra, Harvard Apparatus, Holliston, MA), effectively reducing the ethanol concentration to 25% upon leaving the micromixer. Flow rates were set at 0.5 mL/min for the lipid/ethanol stream and 1.5 mL/min for the siRNA/aqueous stream to drive the solutions through the micromixer at a combined flow rate of 2 mL/min. Previous studies from this laboratory have investigated the effect of flow rate on the size and polydispersity of LNP generated by microfluidics.⁴ It was determined that while increasing the total flow rate from 0.02 to 4 mL/min leads to a progressive decrease in the polydispersity of the LNP, the size of the LNP remains constant at flow rate above 0.2 mL/min. The lipid mixture was then dialyzed for 4 h against 1000 volumes of 50 mM MES/50 mM sodium citrate buffer (pH 6.7) followed by an overnight dialysis against 1000 volumes of 1 \times phosphate buffered saline, pH 7.4 (GIBCO, Carlsbad, CA), using Spectro/Por dialysis membranes (molecular weight cutoff 12 000–14 000 Da, Spectrum Laboratories, Rancho Dominguez, CA).

The mean diameter of the LNP after dialysis was determined by dynamic light scattering (number mode; Zetasizer Nano ZS, Malvern Instruments Inc., Westborough, MA). Lipid concentrations were determined by measuring total cholesterol using the Cholesterol E enzymatic assay from Wako Chemicals USA (Richmond, VA). Encapsulation efficiencies were measured by determining unencapsulated siRNA by measuring the fluorescence upon the addition of RiboGreen (Molecular Probes, Eugene, OR) to the siRNA–LNP (Fi) and comparing this value to the total siRNA content that is obtained upon lysis of the LNP by 1% Triton X-100 (Ft): % encapsulation = $(Ft - Fi)/Ft \times 100$.

2.3. Encapsulation of Gold Nanoparticles. Negatively charged gold nanoparticles (Au-NP) with a diameter 5 nm and surface charge of -55.8 mV were purchased from Ted Pella, Inc., and were used without further purification. LNP were prepared by mixing appropriate volumes of lipid stock solutions in ethanol buffer with an aqueous phase containing Au-NP employing a microfluidic micromixer. An appropriate amount of Au-NP was dissolved in 25 mM sodium acetate buffer, pH 4.0, to achieve a final Au-NP-to-lipid ratio of 2.2×10^{13} particles/ μmol lipid. Lipid dissolved in ethanol and 3 volumes of Au-NP suspended in buffer were combined in the microfluidic micromixer using a dual-syringe pump (PHD Ultra, Harvard Apparatus, Holliston, MA), effectively reducing the ethanol concentration to 25% upon leaving the micromixer. Flow rates were set at 0.5 mL/min for the lipid/ethanol stream and 1.5 mL/min for the aqueous stream to drive the solutions through the micromixer at a combined flow rate of 2 mL/min. A herringbone micromixer⁸ was employed. The resulting formulation was then dialyzed for 4 h against 1000 volumes

of 50 mM MES/50 mM sodium citrate buffer (pH 6.7) followed by an overnight dialysis against 1000 volumes of 1 \times phosphate buffered saline, pH 7.4 (GIBCO, Carlsbad, CA), using Spectro/Por dialysis membranes (molecular weight cutoff 12 000–14 000 Da, Spectrum Laboratories, Rancho Dominguez, CA).

2.4. Cryo-TEM. Cryo-TEM samples were prepared by applying 3 μL of LNP at 10–20 mg/mL total lipid to a standard electron microscopy grid with a perforated carbon film. Excess liquid was removed from the grid by blotting, and then the grid was plunge-frozen in liquid ethane to rapidly freeze the sample using a Vitrobot system (FEI, Hillsboro, OR). Images were taken under cryogenic conditions ($\sim 88\text{K}$) at a magnification of 50 000 \times with an AMT HR CCD camera. Samples were loaded with a Gatan 70 $^\circ$ cryo-transfer holder in an FEI G20 Lab6 200 kV TEM (FEI, Hillsboro, OR) under low dose conditions with an underfocus of 4–6 μm to enhance image contrast. Experiments were performed at the University of British Columbia Bioimaging Centre (Vancouver, BC). Particle diameters were measured from the micrographs with the aid of ImageJ (National Institutes of Health, Bethesda, MD). Average diameters and standard deviations were calculated from more than 100 particles.

3. RESULTS

3.1. Core Nanostructure of LNP Systems Produced by Microfluidic Mixing Is Dependent on Lipid Composition.

The electron dense core of LNP–siRNA systems composed of DLin-KC2-DMA/DSPC/Chol/PEG-lipid (40/11.5/47.5/1; mol/mol) has been attributed to the ability of the cationic lipid/DSPC/cholesterol mixture to form inverted micellar nanostructures, some of which contain siRNA, inside the LNP.⁶ Previous work has also shown that the electron dense core is independent of the presence of siRNA, indicating that the cationic lipid/DSPC/cholesterol lipid system can form inverted micellar nanostructures with an aqueous interior in the absence of siRNA. In addition, other work from this laboratory has shown that LNP formed using a different mixing technique but containing similar lipids (with a higher proportion of DSPC) can exhibit a multilamellar nanostructured core as visualized by cryo-TEM.⁷ It is therefore of interest to determine the influence of lipid composition on LNP nanostructure formed using the microfluidic mixing process to characterize the continuum of structures possible.

As shown in Figure 1A, LNP formed from DLin-KC2-DMA/DSPC/Chol/PEG-lipid (40/11.5/47.5/1; mol/mol) exhibit the characteristic electron dense interior as observed by cryo-TEM. The cationic lipid DLin-KC2-DMA, which has a pK_a of 6.7, was chosen because it exhibits excellent transfection properties following iv administration.³ If the amount of cationic lipid is reduced by 20 mol % and the proportion of (bilayer-forming) DSPC increased by 20 mol % (corresponding to a lipid composition DLin-KC2-DMA/DSPC/Chol/PEG-lipid (20/31.5/47.5/1; mol/mol)), lamellar structures start to comprise the outermost layer of the LNP, while the interior remained solid core (Figure 1B). This behavior suggests that more hydrophobic lipid aggregates may first serve as nucleating sites, possibly containing a higher proportion of DLin-KC2-DMA, that are subsequently coated with lipids containing a higher proportion of DSPC, leading to bilayer structures.

An alternative way of increasing the propensity of component lipids to adopt a lamellar organization is to decrease the unsaturation of acyl chains in component lipids.

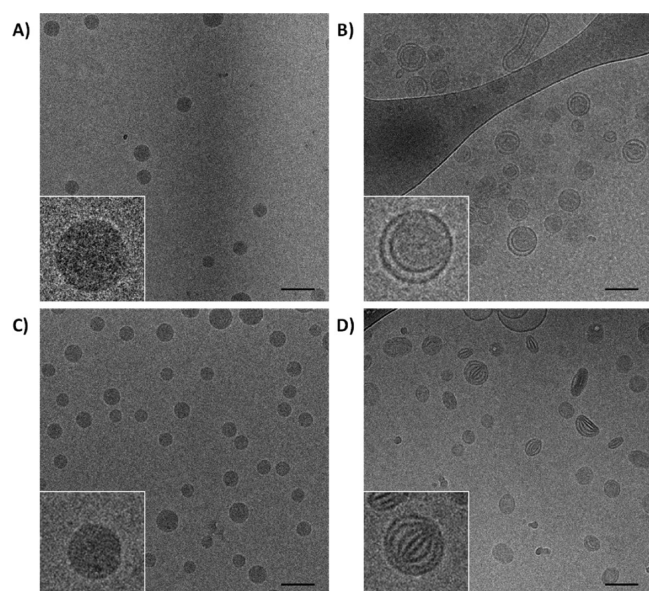


Figure 1. Cryo-TEM micrographs of LNP produced with different cationic lipid saturation and total cationic lipid content: (A) LNP prepared with DLin-KC2-DMA/DSPC/Chol/PEG-lipid (40/11.5/47.5/1; mol/mol); (B) LNP with lipid composition DLin-KC2-DMA/DSPC/Chol/PEG-lipid (20/31.5/47.5/1; mol/mol); (C) LNP with lipid composition DO-KC2-DMA/DSPC/Chol/PEG-lipid (40/11.5/47.5/1; mol/mol); (D) DO-KC2-DMA/DSPC/Chol/PEG-lipid (20/31.5/47.5/1; mol/mol). Scale bar = 100 nm.

In particular, the linoleic acid composition of DLin-KC2-DMA may be expected to contribute to a pronounced “cone” shape driving formation of inverted micellar structure. Decreasing the unsaturation will reduce this structural preference and promote the formation of bilayer structure.⁹ We therefore examined the morphology of LNP systems formed from the oleic acid analogue of DLin-KC2-DMA, namely DO-KC2-DMA. As shown in Figure 1C, LNP containing 40% DO-KC2-DMA exhibits an electron dense interior, similar to LNP containing DLin-KC2-DMA. However, when the DO-KC2-DMA is reduced to 20 mol % and the DSPC content increased to 31.5 mol %, a significant portion of the LNP exhibit morphology consistent with bilayer nanostructures (Figure 1D). It should be noted that the proportion of LNP exhibiting putative bilayer morphology is greater for LNP containing DO-KC2-DMA and 31.5% DSPC (Figure 1D) than in the LNP containing DLin-KC2-DMA and 31.5% DSPC (Figure 1B), consistent with a decreased ability of the DO-KC2-DMA to induce inverted micellar structures.

3.2. LNP siRNA Systems Containing Higher Levels of siRNA Exhibit Reduced Lamellar Structure. The siRNA content of LNP–siRNA systems may also be expected to influence LNP structure. In particular, it may be expected that siRNA will induce inverted micellar structure in combination with unsaturated cationic lipids due to charge association between the negatively charged oligonucleotide and the positively charged lipids. Further, it is likely that these hydrophobic structures would be among the first to precipitate out of solution as the polarity of the medium increases during

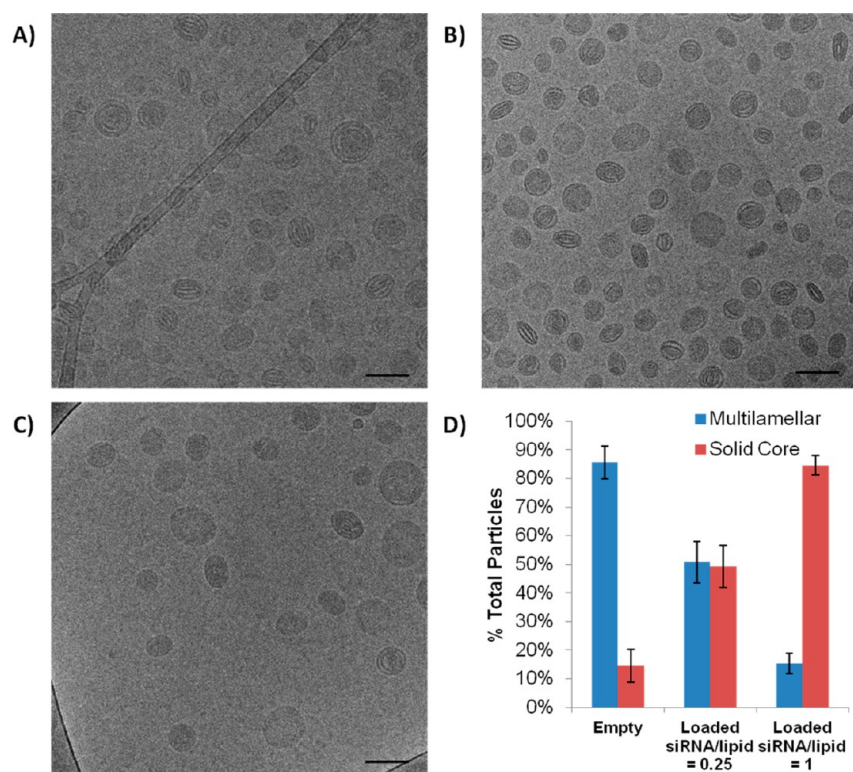


Figure 2. LNP formulated with 20% DO-KC2-DMA exhibit a varying proportion of multilamellar structures depending on siRNA content. (A) Cryo-TEM of LNP composed of DO-KC2-DMA/DSPC/Chol/PEG-c-DMA (20/31.5/47.5/1 mol %) formulated in the absence of siRNA. (B) LNP with the same lipid composition as in (A) but with siRNA at a siRNA/lipid charge ratio of 0.25. (C) LNP with the same lipid composition as in (A) and (B) but prepared with siRNA at siRNA/lipid charge ratio of 1. (D) Particles from cryo-TEM of each sample were counted manually and visually classified into multilamellar or solid core particles. Scale bar = 100 nm.

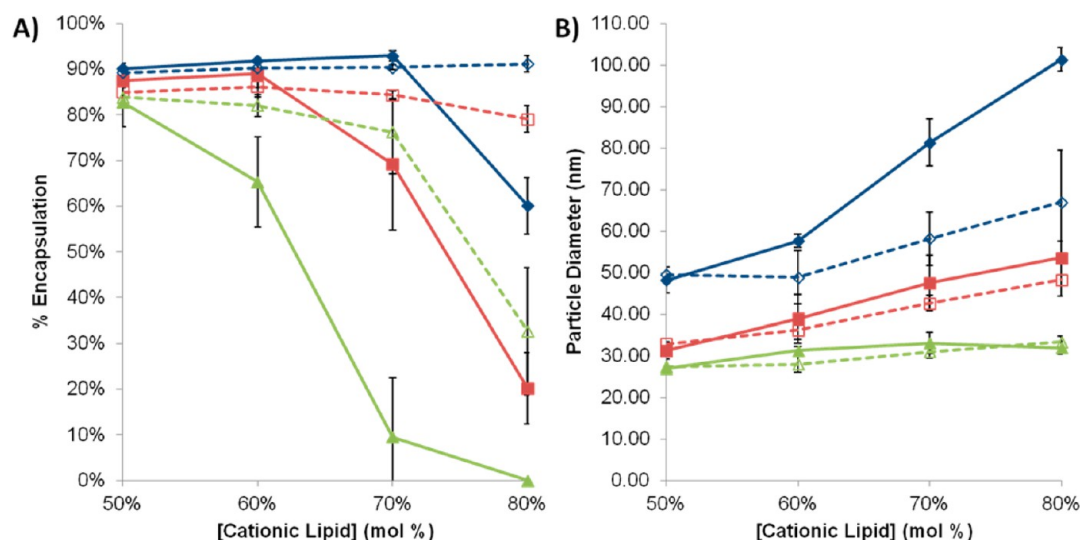


Figure 3. Effects of cationic lipid and phospholipid contents on the siRNA encapsulation efficiency of lipid nanoparticle systems. (A) LNP were formulated using 1% (blue), 2.5% (red), and 5% (green) PEG-*c*-DMA with varying amounts of DLin-KC2-DMA and cholesterol. Formulations were prepared using either 11.5% DSPC (solid lines) or 11.5% DOPE (dashed lines). All formulations were prepared at a siRNA/lipid charge ratio of 0.25. Measurements of encapsulation efficiency were made using the RiboGreen Assay. (B) Particle size of the corresponding LNP formulations in (A). Particle size was reported as the number-weighted mean measured using the Malvern ZetaSizer.

the microfluidic mixing process, thus serving as nucleation sites for LNP formation. If this is the case then it would be expected that the presence of siRNA should enhance the formation of solid core morphology. The structure of LNP composed of DO-KC2-DMA/DSPC/Chol/PEG-lipid (20/31.5/47.5/1; mol/mol) that contained siRNA at siRNA-to-cationic lipid charge ratios of 0, 0.25, and 1 were therefore investigated employing cryo-TEM. As shown in Figure 2, as the siRNA/lipid charge ratio was increased, the proportion of particles displaying bilayer structure in the population of LNP decreased from nearly 90% when no siRNA is present to less than 10% at a siRNA/cationic lipid charge ratio of 1. This supports the proposal that electrostatic interactions between cationic lipids and siRNA provide a strong driving force for the formation of inverted micellar structures surrounding siRNA duplexes, leading to the uniformly electron dense core of the LNP.

3.3. Reduced LNP siRNA Encapsulation Efficiencies Observed at High Cationic Lipid Contents Can Be Improved by Incorporation of DOPE. The ionizable cationic lipids contained in the LNP–siRNA systems described here serve two functions: first to allow efficient encapsulation of siRNA and second to facilitate efficient endosomal escape following uptake into target cells. As shown elsewhere,¹⁰ the gene silencing potency of LNP–siRNA systems depends crucially on the pK_a of the ionizable cationic lipid, a feature that has been attributed to the need to generate positively charged lipids (at endosomal pH values) that can combine with endogenous anionic lipids to disrupt the endosome and release encapsulated siRNA. In this context it is potentially advantageous to increase the proportion of cationic lipid in the LNP to achieve maximal endosomal escape and gene silencing potency. We therefore investigated the effects of increasing the proportions of DLin-KC2-DMA in LNP containing DLin-KC2-DMA, DSPC, cholesterol and PEG-*c*-DMA. The LNP were prepared with DSPC and PEG-*c*-DMA held constant at 11.5% and 1%, respectively, while the DLin-KC2-DMA content was increased from 50% to 80% with the cholesterol content decreased proportionally. All formulations were prepared at a

constant siRNA/cationic lipid charge ratio of 0.25. Surprisingly, siRNA encapsulation efficiencies dropped dramatically as the DLin-KC2-DMA content was increased beyond 70% (Figure 3A), and this effect was even more pronounced when the formulation contained higher percentages (2.5% or 5%) of PEG lipid. It may also be noted that the LNP size increased as the cationic lipid content was increased (Figure 3B).

As noted elsewhere,⁴ higher PEG lipid contents lead to smaller LNP as the PEG lipid is located preferentially on the LNP exterior, leading to higher surface to volume ratios for higher PEG contents and correspondingly smaller sizes. The sizes of LNP–siRNA systems containing 50 mol % cationic lipid and 1, 2.5, and 5 mol % PEG lipid were 46.2, 31.1, and 26.9 nm as measured by dynamic light scattering (number mode), consistent with previous observations. The reduction in trapping efficiencies at higher PEG lipid contents could arise, at least in part, due to the larger surface-to-volume ratios of the smaller LNP systems, leading to a larger proportion of cationic lipid on the surface where any associated siRNA would be exposed. However, this cannot be the complete picture because for a given PEG lipid content an increase in cationic lipid content can dramatically decrease trapping efficiencies without a significant change in size. For example, for a DLin-KC2-DMA formulation containing 5% PEG-lipid, increasing the DLin-KC2-DMA content from 50% to 80% decreased siRNA encapsulation efficiencies from 80% to 0 (Figure 3A); however, the LNP size did not change significantly.

Another reason for low encapsulation efficiencies at high cationic lipid contents could be that the packing properties of components lipids at higher cationic lipid contents do not facilitate encapsulation. For example, it can be estimated¹¹ that the dimensions of the siRNA duplexes are 2.6 nm in diameter and 5.8 nm in length, corresponding to a surface area of approximately 31 nm². If each of the cationic lipids associated with the siRNA are associated with a negative charge, one would expect 42 cationic lipids per siRNA. Although the area per molecule (A_m) in the headgroup region of the ionizable cationic lipids is unknown, it would not be expected to be

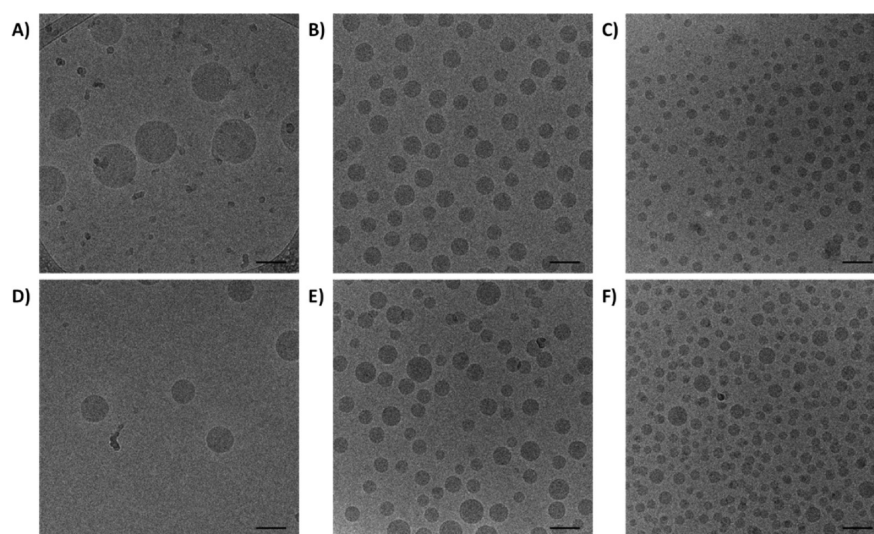


Figure 4. LNP–siRNA systems with high cationic lipid contents maintain solid core structures when formulated with both DSPC and DOPE. (A–C) Cryo-TEM of LNP composed of DLin-KC2-DMA/DSPC/cholesterol/PEG-c-DMA at a ratio of (A) 80/11.5/7.5/1 (mol %), (B) 80/11.5/6/2.5 (mol %), and (C) 80/11.5/3.5/5 (mol %). (D–F) Cryo-TEM of LNP with the same composition as (A), (B), and (C), respectively, but DSPC was replaced with DOPE. All LNP–siRNA systems were formulated at an siRNA/lipid charge ratio of 0.25. Scale bar = 100 nm.

greater than observed for unsaturated diacyl PCs which have A_m values of approximately 0.6 nm^2 ,¹² suggesting that 42 cationic lipids may not be sufficient to cover the surface of the siRNA, requiring additional lipids such as DSPC or cholesterol to form the lipid shell surrounding the siRNA. At the high cationic lipid contents employed here the cholesterol content is correspondingly low. DSPC would not be expected to pack well in the inverted micellar environment surrounding the siRNA and therefore packing constraints may inhibit encapsulation at higher cationic lipid contents. In this regard a lipid such as DOPE, which has a pronounced cone shape compatible with hexagonal H_{II} organization,⁹ may provide improved packing properties. We therefore examined the siRNA trapping efficiencies achieved at high cationic lipid contents when DSPC was replaced by DOPE. As shown in Figure 3A, the siRNA encapsulation efficiencies of LNP formulations containing DOPE in place of DSPC were considerably improved. For formulations with 1% PEG-c-DMA, the substitution of DOPE completely prevented reduced encapsulation efficiencies at high cationic lipid content. Substantial improvements were also observed for formulations containing either 2.5% or 5% PEG-c-DMA.

It is of interest to characterize the structural features of the LNP–siRNA systems at high cationic lipid contents. The structure of LNP prepared with 80% DLinKC2-DMA containing either DSPC or DOPE was examined by cryo-TEM; however, replacing DSPC with DOPE did not alter the structure of the resulting LNP. As shown in Figure 4, both DSPC and DOPE-containing LNP exhibit an electron-dense core, similar to the structure of LNP prepared at lower cationic lipid content.

3.4. Microfluidic Mixing Can Be Used To Encapsulate Large Nucleic Acid Polymers Such as Plasmids and mRNA into LNP Systems. It is of interest to determine whether the microfluidic mixing method for formulating LNP–siRNA systems can be extended to encapsulation of much larger nucleic acid polymers such as mRNA and plasmids. Encapsulation of representative plasmid (pCI-neo-eGFP, 6 kb) and mRNA (1.7 kb, expressing firefly luciferase) constructs was

determined using the same microfluidic mixing protocol as employed for siRNA, in combination with the lipid mixture DLin-KC2-DMA/phospholipid/cholesterol/PEG-c-DMA. The encapsulation efficiencies for each polyanion were compared at two cationic lipid concentrations, 50% versus 80% DLin-KC2-DMA with either DSPC or DOPE in the formulation. As shown in Figure 5, both plasmids and mRNA can be efficiently encapsulated in 50% DLin-KC2-DMA LNP systems, achieving over 70% encapsulation efficiency for plasmid DNA and 90% for mRNA. Increasing the DLin-KC2-DMA content to 80 mol % resulted in reduced encapsulation efficiencies, similar to the behavior exhibited for encapsulation of siRNA. Substitution of DOPE for DSPC in the high cationic lipid formulation resulted in (limited) improvement in encapsulation.

As noted in Figure 6, an interesting feature of cryo-TEM micrographs of plasmid- or mRNA-containing LNP prepared with DSPC is the “bleb” structure appearing on approximately 50% of LNP–plasmid and 20% of LNP–mRNA systems. When the same formulation was prepared with DSPC replaced by DOPE, the protrusions disappeared, and the LNP became uniformly spherical, solid core particles. The fact that the protrusion is only observed in the presence of DSPC suggests that in formulations containing plasmid or mRNA, DSPC can be segregated from other lipid components, possibly forming a bilayer membrane bleb containing an aqueous compartment. This leaves the lipids that are more compatible with inverted micellar or related structures, such as DLin-KC2-DMA and cholesterol, to form the electron-dense portion of the particle in association with the nucleic acids. This interpretation is supported by the fact that when DOPE, which favors the hexagonal H_{II} phase structure in isolation, is substituted for DSPC, no blebs are observed.

3.5. Gold Nanoparticles Can Be Encapsulated in LNP Systems Employing Microfluidic Mixing Techniques. Given the success of microfluidic mixing techniques for encapsulating large polymers such as plasmids and mRNA, it is of obvious interest to try to extend the protocol to larger negatively charged objects such as gold nanoparticles (AuNP). Negatively charged gold nanoparticles (5 nm diameter) were

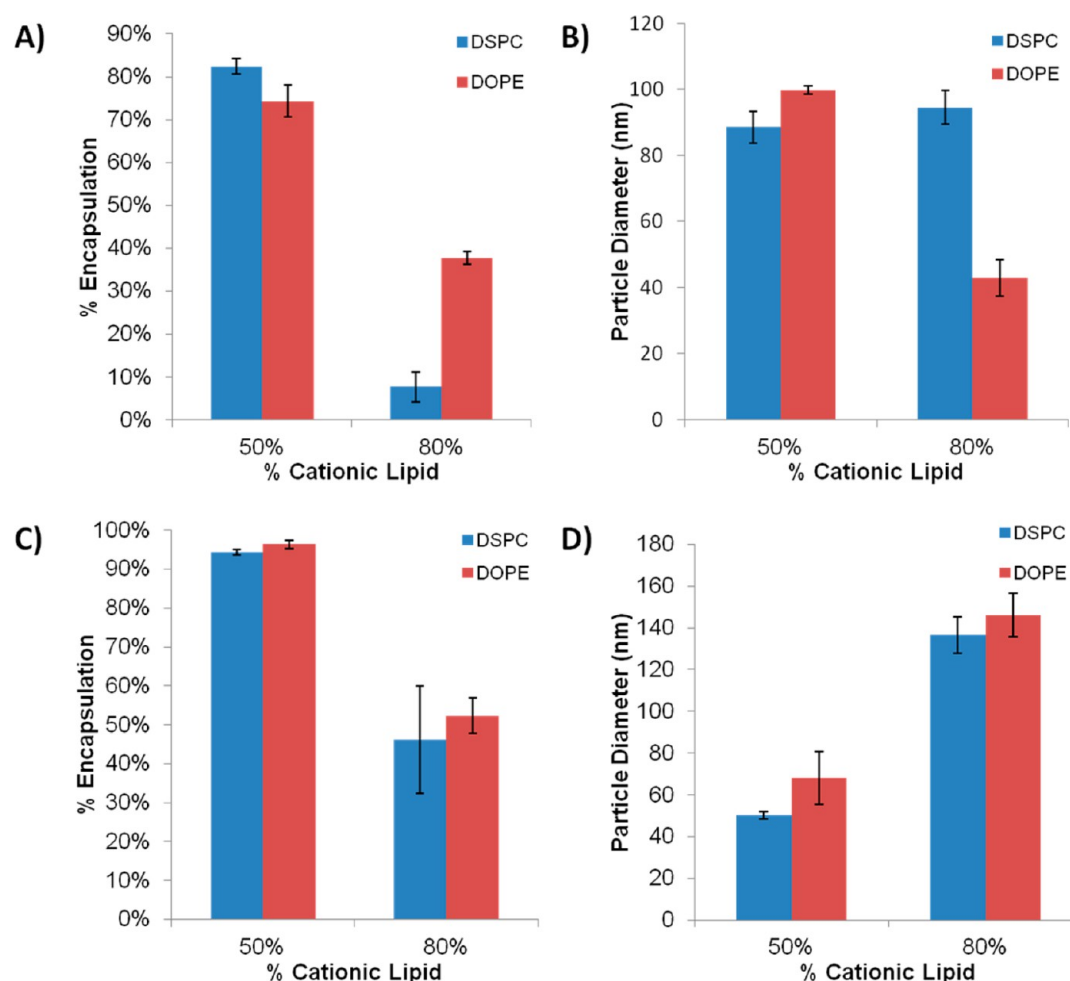


Figure 5. Influence of cationic lipid content and phospholipid species on the plasmid and mRNA encapsulation efficiencies of lipid nanoparticle systems. (A) Plasmid encapsulation efficiency of LNP prepared with DLin-KC2-DMA/phospholipid/cholesterol/PEG-c-DMA at a molar ratio of 50/11.5/37.5/1 or 80/11.5/7.5/1. Formulations were prepared using either DSPC or DOPE as the phospholipid. Measurements of encapsulation efficiency were made using the RiboGreen Assay. (B) Number-based average particle size of the LNP plasmid as measured by dynamic light scattering. (C) Messenger RNA encapsulation efficiency of LNP prepared with the same lipid composition as in (A). All formulations were prepared at a mRNA/lipid charge ratio of 0.25. Measurements of encapsulation efficiency were made using the RiboGreen Assay. (D) Number-based average particle size of the LNP–mRNA as measured by dynamic light scattering.

mixed (using microfluidic mixing) with the lipid mixture DLin-KC2-DMA/DSPC/Chol/PEG-lipid (40/11.5/47.5/1; mol/mol) at an AuNP-to-lipid ratio of 2.2×10^{13} particles/ μmol lipid, and the resulting particles were examined employing cryo-TEM. The resulting LNP systems had an average size of 51.6 ± 8.5 nm as measured by cryo-TEM and exhibited a solid core interior featuring intensely electron-dense dots corresponding to the entrapped gold nanoparticles (Figure 7A). This “currant bun” morphology provides strong support for the nanostructured core model suggested previously by experimental results and by molecular modeling.⁶

It is clear from the electron micrograph that some LNP contain a “bleb” structure surrounding a less electron dense interior (Figure 7A, inset). However, if the DSPC in the lipid mixture was replaced with DOPE, the “blebbing” disappeared and the LNP became spherical (Figure 7B). It is important to note that LNP containing siRNA produced with the identical lipid composition as for Figure 7A do not display bleb structures.⁶ As for LNP containing mRNA and plasmid DNA, it is likely that encapsulation of these highly negatively charged gold nanoparticles triggers segregation of the bilayer-forming

DSPC into the bleb structure. The fact that these “blebs” disappear upon replacing DSPC by DOPE further supports this hypothesis.

4. DISCUSSION

The results presented here show that LNP–siRNA systems can exist in a continuum of bilayer and “solid” electron dense structures depending on the lipid and siRNA content, that siRNA encapsulation efficiencies are compromised at high cationic lipid contents, and that the microfluidic mixing technique can be employed to efficiently encapsulate materials as diverse as mRNA, plasmid DNA, and gold nanoparticles into LNP systems. There are three areas that warrant further discussion, namely the relation between the structural preferences of component lipids and LNP morphology; the role of lipid packing as it relates to siRNA trapping efficiencies; and finally the structure and utility of LNP systems containing mRNA, plasmid DNA, and gold nanoparticles. We discuss these areas in turn.

The studies presented demonstrate that the morphology of LNP formulations of siRNA produced by microfluidic mixing is

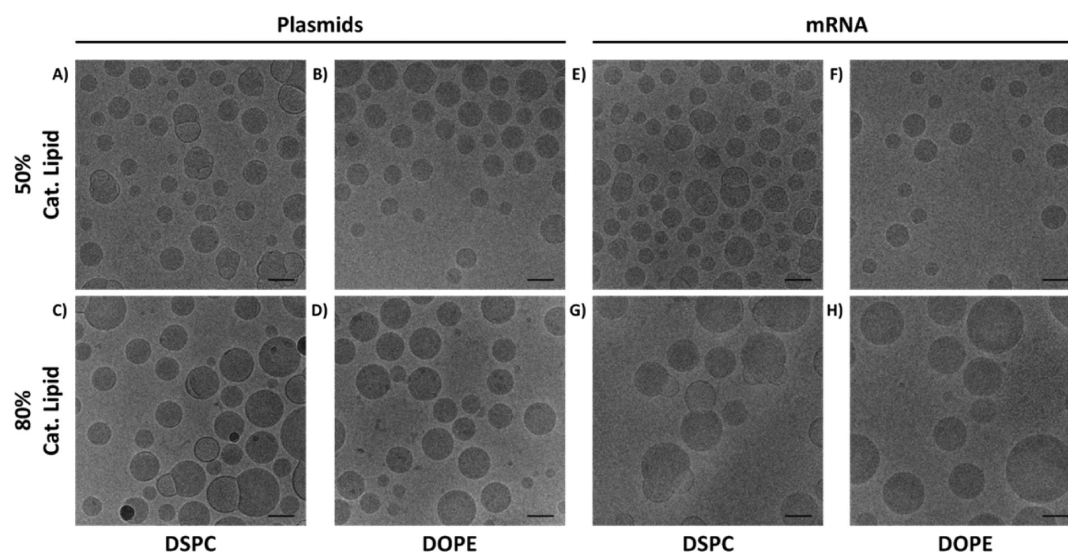


Figure 6. LNP containing plasmid DNA and mRNA exhibit blebs when DSPC is present but not when DOPE is substituted for DSPC. (A, B) Cryo-TEM of LNP–plasmid DNA prepared with the lipid composition DLin-KC2-DMA/phospholipid/Chol/PEG-c-DMA (50/11.5/37.5/1 mol %) with the phospholipid being either (A) DSPC or (B) DOPE. (C, D) Cryo-TEM of LNP–plasmid DNA prepared with the lipid composition DLin-KC2-DMA/phospholipid/Chol/PEG-c-DMA (80/11.5/7.5/1 mol %) with the phospholipid being either (C) DSPC or (D) DOPE. All LNP–plasmid DNA systems were prepared at a plasmid DNA/lipid charge ratio of 0.17. (E–H) Cryo-TEM of LNP with the same lipid composition as (A) to (D), respectively, but prepared with mRNA at a mRNA/lipid charge ratio of 0.25. Scale bar = 100 nm.

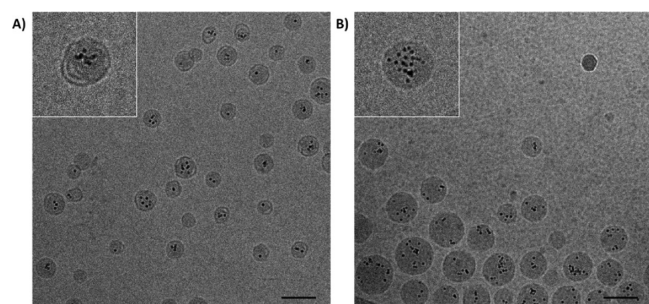


Figure 7. Cryo-TEM of LNP produced with negatively charged gold nanoparticles. (A) LNP prepared with DLin-KC2-DMA/DSPC/Chol/PEG-lipid (40/11.5/47.5/1; % mol) at an Au-NP-to-lipid ratio of 2.2×10^{13} particles/ μmol lipid. (B) LNP prepared with DLin-KC2-DMA/DOPE/Chol/PEG-lipid (40/11.5/47.5/1; % mol) at an Au-NP-to-lipid ratio of 2.2×10^{13} particles/ μmol lipid. Scale bar = 100 nm.

highly dependent on the proportions of component lipids as well as the amount of siRNA encapsulated. The appearance of a proportion of apparently bilayer structure as the amount of DSPC is increased or the unsaturation of the cationic lipid is decreased suggests that the uniformly electron dense interior of LNP–siRNA systems observed for high (40 mol % or more) contents of DLin-KC2-DMA and low (11.5 mol %) proportions of DSPC⁶ represents one extreme of LNP–oligonucleotide organization with an interior consisting of inverted micelles (Figure 8A), whereas the other extreme is small multilamellar systems consisting of concentric bilayers as observed for a lipid composition containing low (20 mol %) levels of cationic lipid and high (25 mol %) levels of DSPC.¹³ As shown here at low levels of cationic lipid (20 mol %) and high (31.5 mol %) levels of DSPC, significant bilayer structure in the LNP–siRNA systems is observed in combination with electron-dense regions. The differences between the structures observed here at low cationic lipid and high DSPC contents as compared to previous work¹³ can be attributed to the different mode of sample preparation, the use of a more saturated

cationic lipid in the Semple study,¹³ and the entrapment of antisense oligonucleotides as compared to siRNA. In particular, the more pronounced electronegativity of double-stranded siRNA as compared to single-stranded DNA may more effectively drive formation of inverted micellar structure.

The observation that siRNA trapping efficiencies decrease dramatically when the cationic lipid content is increased to 80 mol %, and the cholesterol content is decreased to 7.5 mol % is counterintuitive as it could be expected that a higher concentration of positive charge should more readily accommodate siRNA during the encapsulation process. The fact that siRNA encapsulation efficiencies can be rescued by substituting DOPE for DSPC suggests that packing problems of component lipids around the siRNA duplex due to reduced cholesterol levels may lead to the poor encapsulation efficiencies observed. In this picture reduced levels of cholesterol, which has a “cone shape” in the sense that it induces nonbilayer inverted hexagonal H_{II} phases, are compensated for by the presence of DOPE, which has a pronounced cone shape.¹⁴

The ability of microfluidic mixing techniques to enable the efficient encapsulation of mRNA and plasmid DNA in LNP systems clearly provides well-defined delivery systems of considerable interest for promotion of gene expression as opposed to gene silencing. Previous work has shown that mRNA can be encapsulated inside preformed cationic vesicles using protamine to condense mRNA.¹⁵ As shown here, microfluidic mixing techniques do not require nucleic acid-condensing agents such as protamine and result in encapsulation efficiencies of over 90% for LNP–mRNA systems of 70 nm diameter or smaller. It is expected that these LNP–mRNA systems will display similar biodistribution and pharmacokinetic properties as LNP–siRNA systems with the same lipid compositions.¹⁶

It is of interest to ascertain the number of mRNA or plasmid molecules encapsulated per LNP. For siRNA encapsulated in LNP composed of DLin-KC2-DMA/phospholipid/cholester-

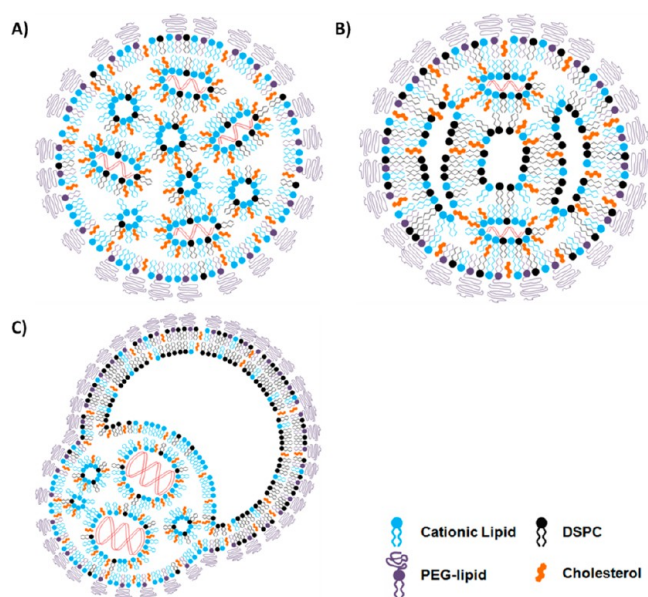


Figure 8. Potential morphologies of LNP–nucleic acid systems. (A) For LNP–siRNA systems containing high cationic lipid content, cationic lipids are preferentially associated with the siRNA due to electrostatic interactions, together with cholesterol and possibly a small proportion of DSPC they form inverted micelles around the siRNA. In addition, excess cationic lipid, cholesterol, and possibly a small proportion of DSPC form “empty” inverted micelles. These aggregated inverted micelles are coated by a layer of PEG lipid, DSPC, and cholesterol. It is possible that the proportion of DSPC is enhanced in this monolayer. (B) LNP–siRNA systems prepared with lower cationic lipid content and a higher proportion of the bilayer-forming DSPC result in formation of some inverted micelles primarily consisting of cationic lipid and cholesterol; DSPC is preferentially located in bilayer regions. (C) For LNP containing longer nucleic acids, such as mRNA or plasmid DNA, cationic lipid is primarily associated with the mRNA or DNA to form solid core structures and the bilayer-forming DSPC is largely segregated into bilayer “bleb” structures.

ol/PEG-c-DMA (50/11.5/37.5/1; mol/mol) at a charge ratio (siRNA negative charge to cationic lipid) of 0.25, it can be calculated that an LNP of 50 nm diameter will contain approximately 200 siRNA molecules. For the mRNA (1.7 kb) encapsulated here at an mRNA to cationic lipid charge ratio of 0.25 a similar calculation reveals that a 50 nm LNP will contain approximately 5 mRNA molecules. Alternatively, for a 6 kb plasmid a 50 nm LNP will contain just one plasmid. At a charge ratio of one the numbers of siRNA, mRNA, and plasmid per 50 nm LNP increase to approximately 850, 20, and 3.

With regard to the structural features of LNP containing mRNA and plasmid DNA, the appearance of apparently bilayer “blebs” on the LNP systems containing DSPC suggests the segregation of bilayer-preferring lipids such as DSPC in such regions (Figure 8C). Interestingly, such blebs are not observed for LNP containing siRNA at similar charge ratios, suggesting that the interior nanostructure packing of lipid around the shorter siRNA oligonucleotides does not lead to such segregation as readily. For an equal number of negative charges, a difference between the siRNA oligonucleotides and the longer mRNA and plasmids is that there are more “ends” in the siRNA, leading to a larger effective surface area per base. It may be that this larger area is needed to accommodate neutral molecules such as DSPC and cholesterol, after the association

of cationic lipids with the negatively charged bases. The disappearance of the blebs on substituting DOPE for DSPC is fully consistent with the preference of this lipid for “inverted” structures such as the hexagonal H_{II} phase¹⁴ as even if this lipid is segregated in the mRNA and plasmid containing LNP, it could still adopt electron-dense nonbilayer structures such as inverted micelles.

LNP–mRNA systems have considerable therapeutic potential both *in vitro*¹⁷ and *in vivo*.¹⁸ It will be of interest to determine whether the LNP–mRNA systems developed here exhibit the same apoE-dependent transfection capabilities *in vitro* and *in vivo* as do LNP–siRNA systems employed for transfection of hepatocytes and neurons.^{19,20} The LNP–mRNA systems described here potentially allow systemic (iv) delivery of mRNA with particular potency for tissues such as the liver (hepatocytes).

Moving to the last discussion topic, the ability to encapsulate negatively charged gold nanoparticles in LNP systems as demonstrated in this work is clearly of major interest. It is likely that gold-containing LNP will have considerable utility for cell and tissue imaging due to the high contrast between gold nanoparticles and surrounding environments as well as the relatively low toxicity of colloidal gold preparations.^{21–23} In addition, due to the efficiency with which certain gold nanoparticles can absorb optical light leading to local heating,²⁴ the potential for triggered release of LNP contents is apparent. As noted earlier, the current appearance of gold nanoparticles encapsulated in the LNP (Figure 7) fully supports the nanostructured core model of LNP–siRNA systems presented elsewhere.⁶ For the gold nanoparticle concentration of 2.2×10^{13} particles per μmol lipid employed in these formulations, it can be calculated, assuming an average (non-PEG) lipid molecular weight of 500 and a lipid density of 0.9 that a 50 nm diameter should contain 3 gold nanoparticles. This is consistent with the electron micrographs presented in Figure 7A, where the average LNP diameter is 51.6 ± 8.5 nm and the average number of gold nanoparticles per LNP is 2.4 ± 2.1 . It may be noted that the LNP systems where DOPE has been substituted for DSPC (Figure 7B) contain significantly more gold nanoparticles per LNP. This can be accounted for by the fact that the DOPE-containing LNP are somewhat larger than the DSPC systems, with a mean diameter of 92.7 ± 17.8 nm.

5. CONCLUSIONS

In summary, the results presented here show that the microfluidic mixing technique is a general method for generating well-defined LNP systems containing a large variety of negatively charged macromolecules including mRNA, plasmids, and gold nanoparticles. As demonstrated here for siRNA, the nanostructure of these systems is sensitive to the structural preferences of component lipids, where the balance of bilayer to nonbilayer lipids can modulate a transition from multilamellar to solid core appearance. In addition, the micrographs of LNP containing gold nanoparticles provides additional support for the nanostructured core model of LNP–siRNA systems suggested in previous work. It is envisaged that these systems will have considerable utility as therapeutic agents as well as for imaging applications.

AUTHOR INFORMATION

Corresponding Author

*(P.R.C.) E-mail pieterc@mail.ubc.ca.

Present Address

A.K.K.L.: Department of Chemistry, University of Victoria, British Columbia, Canada V8W 3V6.

Notes

The authors declare the following competing financial interest(s): P.R.C. has a financial interest in Precision NanoSystems Inc. The rest of the authors declare no competing financial interest.

ACKNOWLEDGMENTS

This work is supported by the Canadian Institutes of Health Research team grant FRN111627. Josh Zaifman is gratefully thanked for synthesizing DO-KC2-DMA.

REFERENCES

- (1) Torchilin, V. P. Recent Advances with Liposomes as Pharmaceutical Carriers. *Nat. Rev. Drug Discovery* **2005**, *4*, 145–160.
- (2) Zhang, L.; Chan, J. M.; Gu, F. X.; Rhee, J.; Wang, A. Z.; Radovic-moreno, A. F.; Alexis, F.; Langer, R.; Farokhzad, O. C. Self-Assembled Lipid Polymer Hybrid Nanoparticles: A Robust Drug Delivery Platform. *ACS Nano* **2008**, *2*, 1696–1702.
- (3) Semple, S. C.; Akinc, A.; Chen, J.; Sandhu, A. P.; Mui, B. L.; Cho, C. K.; Sah, D. W. Y.; Stebbing, D.; Crosley, E. J.; Yaworski, E.; et al. Rational Design of Cationic Lipids for siRNA Delivery. *Nat. Biotechnol.* **2010**, *28*, 172–176.
- (4) Belliveau, N. M.; Huft, J.; Lin, P. J.; Chen, S.; Leung, A. K.; Leaver, T. J.; Wild, A. W.; Lee, J. B.; Taylor, R. J.; Tam, Y. K.; et al. Microfluidic Synthesis of Highly Potent Limit-Size Lipid Nanoparticles for In Vivo Delivery of siRNA. *Mol. Ther. Nucleic Acids* **2012**, *1*, e37.
- (5) Zhigaltsev, I. V.; Belliveau, N.; Hafez, I.; Leung, A. K. K.; Huft, J.; Hansen, C.; Cullis, P. R. Bottom-up Design and Synthesis of Limit Size Lipid Nanoparticle Systems with Aqueous and Triglyceride Cores Using Millisecond Microfluidic Mixing. *Langmuir* **2012**, *28*, 3633–3640.
- (6) Leung, A. K. K.; Hafez, I. M.; Baoukina, S.; Belliveau, N. M.; Zhigaltsev, I. V.; Afshinmanesh, E.; Tieleman, D. P.; Hansen, C. L.; Hope, M. J.; Cullis, P. R. Lipid Nanoparticles Containing siRNA Synthesized by Microfluidic Mixing Exhibit an Electron-Dense Nanostructured Core. *J. Phys. Chem. C* **2012**, *116*, 18440–18450.
- (7) Maurer, N.; Wong, K. F.; Stark, H.; Louie, L.; McIntosh, D.; Wong, T.; Scherrer, P.; Semple, S. C.; Cullis, P. R. Spontaneous Entrapment of Polynucleotides upon Electrostatic Interaction with Ethanol-Destabilized Cationic Liposomes. *Biophys. J.* **2001**, *80*, 2310–2326.
- (8) Stroock, A. D.; Dertinger, S. K. W.; Ajdari, A.; Mezic, I.; Stone, H. A.; Whitesides, G. M. Chaotic Mixer for Microchannels. *Science* **2002**, *295*, 647–651.
- (9) Cullis, P. R.; Hope, M. J.; Tilcock, C. P. Lipid Polymorphism and the Roles of Lipids in Membranes. *Chem. Phys. Lipids* **1986**, *40*, 127–144.
- (10) Jayaraman, M.; Ansell, S. M.; Mui, B. L.; Tam, Y. K.; Chen, J.; Du, X.; Butler, D.; Eltepu, L.; Matsuda, S.; Narayanannair, J. K.; et al. Maximizing the Potency of siRNA Lipid Nanoparticles for Hepatic Gene Silencing In Vivo. *Angew. Chem., Int. Ed.* **2012**, *51*, 8529–8533.
- (11) Rosenberg, J. M.; Seeman, N. C.; Day, R. O.; Rich, A. RNA Double Helices Generated from Crystal Structures of Double Helical Dinucleoside Phosphates. *Biochem. Biophys. Res. Commun.* **1976**, *69*, 979–987.
- (12) Alwarawrah, M.; Dai, J.; Huang, J. A Molecular View of the Cholesterol Condensing Effect in DOPC Lipid Bilayers. *J. Phys. Chem. B* **2010**, *114*, 7516–7523.
- (13) Semple, S. C.; Klimuk, S. K.; Harasym, T. O.; Dos Santos, N.; Ansell, S. M.; Wong, K. F.; Maurer, N.; Stark, H.; Cullis, P. R.; Hope, M. J.; et al. Efficient Encapsulation of Antisense Oligonucleotides in Lipid Vesicles Using Ionizable Aminolipids: Formation of Novel Small Multilamellar Vesicle Structures. *Biochim. Biophys. Acta* **2001**, *1510*, 152–166.
- (14) Cullis, P. R.; de Kruijff, B. Lipid Polymorphism and the Functional Roles of Lipids in Biological Membranes. *Biochim. Biophys. Acta* **1979**, *559*, 399–420.
- (15) Wang, Y.; Su, H.-H.; Yang, Y.; Hu, Y.; Zhang, L.; Blancafort, P.; Huang, L. Systemic Delivery of Modified mRNA Encoding Herpes Simplex Virus 1 Thymidine Kinase for Targeted Cancer Gene Therapy. *Mol. Ther.* **2013**, *21*, 358–367.
- (16) Mui, B. L.; Tam, Y. K.; Jayaraman, M.; Ansell, S. M.; Du, X.; Lin, P. J. C.; Chen, S.; Narayanannair, J. K.; Rajeev, K. G.; Manoharan, M.; et al. Influence of Polyethylene Glycol Lipid Desorption Rates on Pharmacokinetics and Pharmacodynamics of siRNA Lipid Nanoparticles. *Mol. Ther. Nucleic Acids* **2013**, *2*, e139.
- (17) Sahin, U.; Karikó, K.; Türeci, Ö. mRNA-Based Therapeutics — Developing a New Class of Drugs. *Nat. Rev. Drug Discovery* **2014**, *13*, 759–780.
- (18) Kormann, M. S. D.; Hasenpusch, G.; Aneja, M. K.; Nica, G.; Flemmer, A. W.; Herber-Jonat, S.; Huppmann, M.; Mays, L. E.; Illenyi, M.; Schams, A.; et al. Expression of Therapeutic Proteins after Delivery of Chemically Modified mRNA in Mice. *Nat. Biotechnol.* **2011**, *29*, 154–157.
- (19) Akinc, A.; Querbes, W.; De, S.; Qin, J.; Frank-kamenetsky, M.; Jayaprakash, K. N.; Jayaraman, M.; Rajeev, K. G.; Cantley, W. L.; Dorkin, J. R.; et al. Targeted Delivery of RNAi Therapeutics with Endogenous and Exogenous Ligand-Based Mechanisms. *Mol. Ther.* **2010**, *18*, 1357–1364.
- (20) Rungta, R. L.; Choi, H. B.; Lin, P. J. C.; Ko, R. W.; Ashby, D.; Nair, J.; Manoharan, M.; Cullis, P. R.; Macvicar, B. A. Lipid Nanoparticle Delivery of siRNA to Silence Neuronal Gene Expression in the Brain. *Mol. Ther. Nucleic Acids* **2013**, *2*, e136.
- (21) Gilleron, J.; Querbes, W.; Zeigerer, A.; Borodovsky, A.; Marsico, G.; Schubert, U.; Manygoats, K.; Seifert, S.; Andree, C.; Stöter, M.; et al. Image-Based Analysis of Lipid Nanoparticle-Mediated siRNA Delivery, Intracellular Trafficking and Endosomal Escape. *Nat. Biotechnol.* **2013**, *31*, 638–646.
- (22) Connor, E. E.; Mwamuka, J.; Gole, A.; Murphy, C. J.; Wyatt, M. D. Gold Nanoparticles are Taken up by Human Cells but Do Not Cause Acute Cytotoxicity. *Small* **2005**, *1*, 325–327.
- (23) Hainfeld, J. F.; Slatkin, D. N.; Focella, T. M.; Smilowitz, H. M. Gold Nanoparticles: A New X-Ray Contrast Agent. *Br. J. Radiol.* **2006**, *79*, 248–253.
- (24) Paasonen, L.; Laaksonen, T.; Johans, C.; Yliperttula, M.; Kontturi, K.; Urtti, A. Gold Nanoparticles Enable Selective Light-Induced Contents Release from Liposomes. *J. Controlled Release* **2007**, *122*, 86–93.